

# Substrate Reshaping for Optically Tuned Liquid-Printed Microlenses Beyond Their Wetting Properties

Ernest Martí Jerez, J. Marcos Fernández Pradas,\* Pere Serra, and Martí Duocastella\*

Several strategies exist capable of fabricating microlenses for applications such as cameras and solar cells. Among them, techniques based on printing curable liquid prepolymers including inkjet and electrohydrodynamic-jet printing, or laser-induced forward-transfer (LIFT) offer unique advantages in terms of ease of integration, cost, and compatibility with flexible substrates. However, the optical properties of the so-fabricated microlenses depend on the wettability of the liquid prepolymer, preventing the broad implementation of printing technologies for micro-optics. Herein, how printing microdroplets on top of reconfigurable substrates allows overcoming this issue is reported. The strategy, called print-n-release, is based on depositing prepolymer microdroplets on top of mechanically stretched elastomeric substrates. Once the stress applied to the substrate is released, and provided pinning of the contact line, the microdroplet's base diameter decreases producing an increase in contact angle and reduction in radius of curvature. Following a curing step, the microdroplets are converted into microlenses whose shape no longer depends exclusively on their wetting properties, but also on the substrate elongation. It is demonstrated that, by combining LIFT with substrates elongated up to 80%, microlenses can be fabricated with a 400% increase in contact angle and a 90% reduction in focal length, in good agreement with theoretical predictions.

scanning speed in optical microscopes,<sup>[6]</sup> or retrieve quantitative phase information in Shack–Hartmann wavefront sensors.<sup>[7]</sup> However, the broad implementation of microlenses is facing a major roadblock: current fabrication techniques fail to accommodate the demands in terms of shape, material, or microlens placement required in flexible optoelectronics,<sup>[8]</sup> integral imaging,<sup>[9]</sup> and other emerging applications. Typically, microlenses are fabricated using lithographic techniques and thermal reflow processes.<sup>[1,10]</sup> Highly reproducible microlenses have been produced via photolithography and electron-beam lithography, but these methods require rigid flat substrates and are incompatible with controlled lens placement.<sup>[11,12]</sup> Soft lithography approaches can be used to directly deposit microlenses of optical polymers, but the fabrication of high-quality molds or masters can be challenging<sup>[13,14]</sup> – in fact, they are normally produced via photolithography and thermal reflow.<sup>[15,16]</sup> Similarly, lithographic approaches can be used to

## 1. Introduction

Microlenses are key components of next-generation optoelectronic systems in fields as relevant as imaging and photovoltaics.<sup>[1,2,3]</sup> They can be used to enhance the photon collection efficiency of photodetectors<sup>[4]</sup> and solar cells,<sup>[5]</sup> increase


generate patterns of micro- and even nanodomains with specific wettability properties for the generation of tunable lenses by flowing different liquids. Still, the inherent problems of lithography prevail.<sup>[17,18]</sup> Additionally, none of these mask-based techniques is optimal for applications requiring small, customized units. An operation apparently as simple as adding a microlens on top of a light-emitting diode or an avalanche photodetector, is not feasible with state-of-the-art lithographic methods.<sup>[19,20]</sup>

Several strategies have been developed to achieve on-demand microlens fabrication on different substrates, including flexible, stretchable, or even microelectronic components. Among them, direct writing techniques (DWTs) based on printing wet materials, such as ink-jet printing,<sup>[21–23]</sup> electrohydrodynamic jet printing,<sup>[24,25]</sup> or laser-induced forward transfer (LIFT),<sup>[26–28]</sup> enable high throughput and high-quality maskless fabrication of microlenses with relatively simple systems. In these cases, a two-step process is usually implemented. First, microdroplets of a UV curable liquid prepolymer are deposited on a substrate. Second, the microdroplets are converted into solid planoconvex microlenses after exposure to UV light. Because surface tension produces droplets with a perfectly spherical-cap shape and very high smoothness, the so-fabricated microlenses exhibit high

E. Martí Jerez, J. M. Fernández Pradas, P. Serra, M. Duocastella  
Department of Applied Physics  
Universitat de Barcelona

C/Martí i Franquès 1, Barcelona 08028, Spain  
E-mail: jmfernandez@ub.edu; marti.duocastella@ub.edu

E. Martí Jerez, J. M. Fernández Pradas, P. Serra, M. Duocastella  
Institute of Nanoscience and Nanotechnology (IN2UB)  
Universitat de Barcelona  
Barcelona 08028, Spain

 The ORCID identification number(s) for the author(s) of this article can be found under <https://doi.org/10.1002/admt.202300564>

© 2023 The Authors. Advanced Materials Technologies published by Wiley-VCH GmbH. This is an open access article under the terms of the Creative Commons Attribution-NonCommercial License, which permits use, distribution and reproduction in any medium, provided the original work is properly cited and is not used for commercial purposes.

DOI: 10.1002/admt.202300564

optical quality.<sup>[29]</sup> However, the microdroplet shape is only determined by the contact angle between prepolymer and substrate. Consequently, the microlens geometry and its optical properties are fixed for a given material and substrate.<sup>[30]</sup> In other words, it is not possible to control the focusing performance of a microlens: the numerical aperture remains fixed, and consequently, the minimum focus spot size and depth-of-field (DOF). While a change in the chemical properties of the substrate can solve this issue, this strategy can be difficult to implement at only selected regions on a substrate, and it can also alter the optimal printing conditions.<sup>[31,32]</sup> Simply put, a method that preserves the core advantages of wet DWTs in terms of maskless fabrication, throughput, and substrate compatibility, while allowing for on-demand control of the microlens shape, does not exist.

In this work, we address this issue and present a novel fabrication process compatible with any wet DWT that allows for microlens fabrication with tuned focusing performance. Our approach, called “print-n-release”, is based on modifying the geometry of printed prepolymer microdroplets by using a reconfigurable substrate. Specifically, we used flexible elastomeric materials subject to different types of stress. Upon release, and provided pinning of the contact line, the microdroplets deform because of substrate shrinking. Following a UV-curable step, the microdroplets can then be converted into microlenses. Notably, this approach allows the decoupling of the final microlens shape from the wetting behavior between prepolymer and substrate. Thus, the optical properties of a microlens for a given lens base diameter are not only given by the liquid-substrate wettability but also by the mechanical strain applied, which effectively plays the role of a new degree of freedom. Here, we describe the fundamentals of the approach and demonstrate its feasibility by printing different microlenses using LIFT. We also perform a detailed analysis of the microlens geometry and their optical properties under different substrate reconfigurations, which is in good agreement with theoretical predictions. As a proof-of-concept, we use the printed microlenses to form images and for enhancing the numerical aperture of an optical system.

## 2. Principle and Implementation of Print-n-Release

The core idea of print-n-release is to use mechanically reconfigurable substrates to fabricate polymeric microlenses whose optical properties can be actively changed beyond the limits imposed by the substrate-prepolymer wettability. In previous studies, shrinkable substrates, stressed elastomers or hydrogels have been successfully used to increase the resolution of some fabrication techniques by diminishing the dimensions of the so-fabricated patterns.<sup>[33–35]</sup> Building from these promising results, print-n-release uses stretched elastomers not only to fabricate microlenses with a small base diameter but to modify the geometrical parameters that dictate optical performance, that is, height, contact angle, and radius of curvature. As shown in **Figure 1a**, our approach is based on depositing UV-curable prepolymer microdroplets on top of an elastomer elongated by an amount  $\epsilon$ , known as the engineering strain. A microdroplet printed on top of such stretched elastomer has a volume:

$$V = \frac{\pi h}{6} (3a^2 + h^2) \quad (1)$$

where  $a$  and  $h$  are the base radius and height of the droplet, respectively. This equation holds if surface tension effects dominate over gravity forces (Bond number smaller than one), which typically occurs for microdroplets with a diameter smaller than 1 mm<sup>[36]</sup> (see Supporting Information Section S2). Assuming perfect pinning of the contact line, upon releasing stress, the droplet's base decreases together with the substrate as:

$$a' = a(1 + \epsilon)^{-1} \quad (2)$$

where  $a'$  is the shrunk droplet radius. Because the droplet volume is preserved – no significant evaporation occurs at room temperature for most common liquid prepolymers – such a change results in an increase in the droplet's height  $h'$ . Note that such a droplet will also feature a Bond number much smaller than one, and thus exhibit an almost perfectly spherical shape. Therefore, the value of  $h'$  can be found by solving the equation:

$$V = \frac{\pi h'}{6} (3a'^2(1 + \epsilon)^{-2} + h'^2) \quad (3)$$

where  $V$  is the initial droplet volume given in Equation 1 (see Supporting Information for a full derivation). Therefore, control of the final microdroplet's shape can be achieved by adjusting the initially applied strain. Once the liquid microdroplet has reached the desired size, it can then be converted into a high-quality solid microlens upon UV exposure.

Figure 1b shows numerical calculations, using the mathematical model described above, of the change in contact angle and paraxial focal length as a function of the substrate engineering strain  $\epsilon$ . Notably, the change in contact angle increases with the applied strain, with droplets featuring a low initial contact angle experiencing a more pronounced change. For instance, a droplet with an initial contact angle of 15° deposited on top of a substrate elongated by a factor of 80%, can reach a final contact angle above 60°. The change in contact angle also affects the optical properties of the droplet. Indeed, as  $\epsilon$  increases, the paraxial focal length decreases. Again, the major changes occur for droplets with an initially low contact angle. In this case, a microdroplet with a 15° contact angle and focal length of 100 µm printed on top of a substrate elongated by a factor of 80%, would achieve, after releasing stress, a focal length of only 15 µm. The non-linear relationship between focal length and base diameter also allows tuning the microlens focusing power, that is, its numerical aperture (NA). In fact, the microdroplet NA in the previous example could increase from 0.1 to 0.7.

To implement print-n-release in practice, it suffices to follow the four-step process schematized in Figure 1c. First, the elastomeric substrate is elongated by applying a controlled stretching stress. In current experiments, we used a lathe chuck that facilitates isotropic stretching. Second, a liquid microdroplet is printed on top of the pre-stretched substrate. To this end, any DWT method ranging from e-jet printing to LIFT could be used. We selected the latter for its compatibility with high-viscosity liquids. Third, the stress responsible for substrate elongation is released. Consequently, the substrate shrinks until recovering its original size. For most common prepolymer-substrate pairs, there is significant pinning of the contact line. Therefore, the shrinking of the substrate also results in a reduction in the

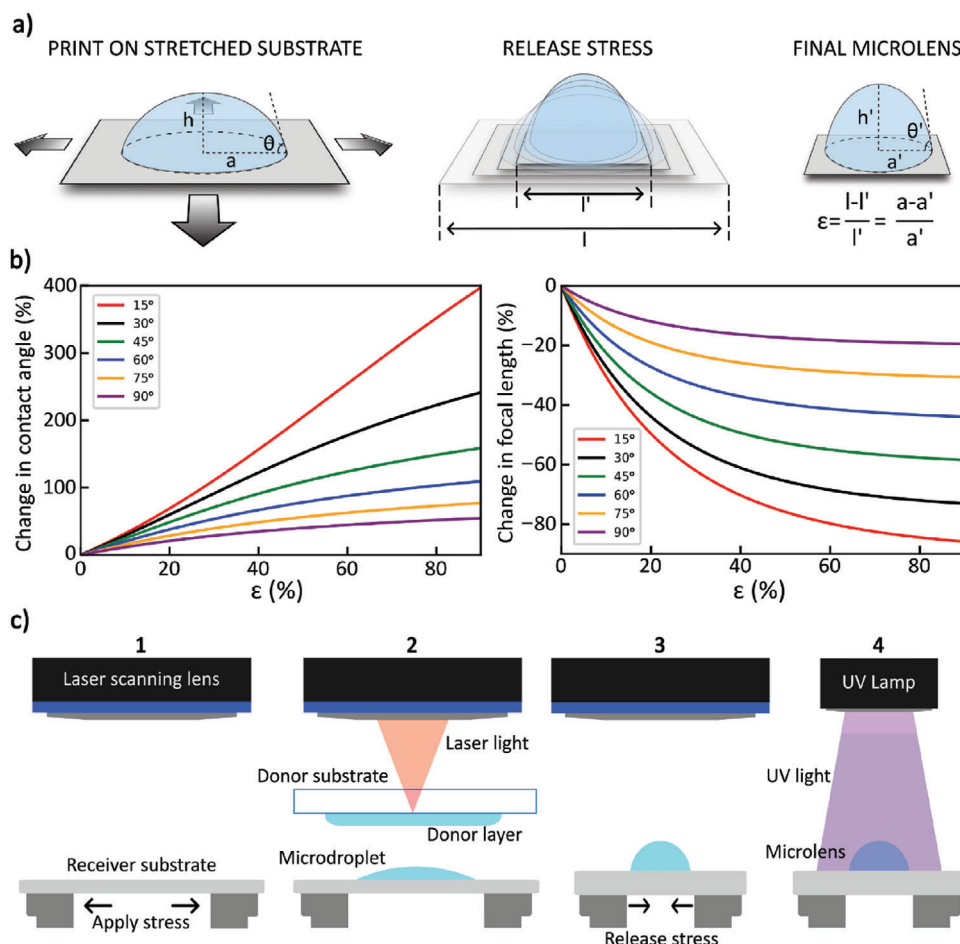


**Figure 1.** Principle and implementation of print-n-release. a) Sketch of a microdroplet printed on top of a stretched substrate. Upon releasing the stress applied to the substrate, and considering pinning of the contact line, the microdroplet experiences a reduction in base diameter and a gain in contact angle and height. b) Plots of the expected change in contact angle and focal length (%) versus  $\epsilon$  (%) for different initial contact angles. c) Scheme of the different steps required to implement print-n-release in practice. First, stress is applied to an elastomeric substrate that results in its elongation. Second, liquid prepolymer microdroplets are printed on top of the substrate using a DWT method (LIFT in current experiments). Third, the stress is released, producing the recovery of the substrate to its initial size and the consequent shrinking of the microdroplet. Four, the microdroplets are solidified via UV light exposure.

microdroplet's base diameter and an increase in its contact angle. During this process, the microdroplet remains in a liquid state. Finally, the microdroplet is converted into a solid microlens by curing the liquid prepolymer under UV light exposure. Note that controlling the initial volume of the printed droplet and substrate elongation allows the fabrication of microdroplets with an identical base diameter and a different focal length, something not possible with conventional DWT methods.

### 3. Morphological Study

As a first step to prove the feasibility of print-n-release, we determined the optimal laser conditions for printing microdroplets of a transparent UV-curable optical glue (our liquid prepolymer in experiments herein). To this end, we performed a parametric study of the dependence of the droplet size with laser pulse energy. As shown in Figure S2 (Supporting Information), a minimum energy of 15  $\mu\text{J}$  is needed to induce printing, above that the

droplet radius increases linearly with laser energy from a minimum value of 30 to 55  $\mu\text{m}$  at 40  $\mu\text{J}$ . Such a behavior, already observed with LIFT of high viscosity inks,<sup>[29]</sup> can be explained by the need to generate a gas bubble with enough pressure to induce jetting of the prepolymer, but below the limit that results in bubble bursting. Importantly, within this parameter window, well-defined droplets with a small contact angle of 15° and diameters ranging from 30 to 55  $\mu\text{m}$  can be printed. Note that obtaining a higher contact angle, which would be beneficial for enhanced focusing, would not be possible without modifying the wettability of the substrate.

Next, we studied the morphological changes of microlenses fabricated on top of pre-stretched substrates with different  $\epsilon$ . In current experiments, we used an acrylic foam tape that allows for elongations of up to 200% without rupture, but similar results can be obtained using common elastomers such as poly-dimethyl-siloxane (PDMS), as reported in the Supporting Information. **Figure 2** shows scanning electron microscopy

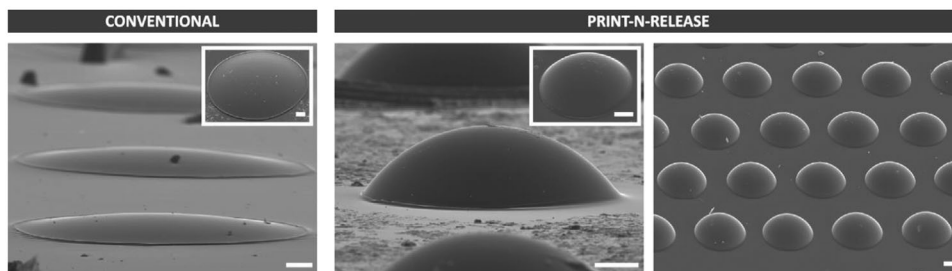


**Figure 2.** SEM images of microlenses fabricated with the conventional approach and using print-n-release with  $\epsilon = 80\%$ . The right image and the insets were captured at a  $45^\circ$  imaging angle, whereas the remaining two images were captured at a  $90^\circ$  imaging angle. Scale bars  $20\ \mu\text{m}$ .

(SEM) images of microlenses fabricated with and without elongation of the substrate. Remarkably, the microlenses generated using print-n-release feature a much higher contact angle. This indicates that pinning of the microdroplets' contact line during substrate shrinking indeed exists, which in turn validates our overall approach.

For a more quantitative analysis, we measured, at different stages upon stress release, the pitch distance between microdroplets arranged in array form. We compared these results with the average radius of the microdroplets, as shown in **Figure 3a**. The linear dependence between pitch and radius indicates that microdroplets shrink together with the substrate, further confirming the pinning of the contact line. Similar results can be obtained by plotting the change in microlens radius relative to

substrate deformation (Figure S3, Supporting Information). In this case, these parameters exhibit a linear relationship with a slope of 0.94, close to the ideal value of 1 corresponding to perfect pinning.

A more detailed study of the change in contact angle for different  $\epsilon$  is shown in **Figure 3b**. In all cases, the final contact angle increases with  $\epsilon$ , in perfect agreement with theoretical predictions – see solid blue line. For instance, microlenses fabricated applying an engineering strain of  $24\%$  have a contact angle of  $25^\circ$  (95% higher than the one obtained as deposited) while those fabricated applying  $\epsilon = 83\%$  have a contact angle of  $61^\circ$  (410% higher than the one obtained as deposited). Such a change also affects the curvature of the microlenses, and consequently, their paraxial focal length (see Supporting Information). **Figure 3c** shows the change

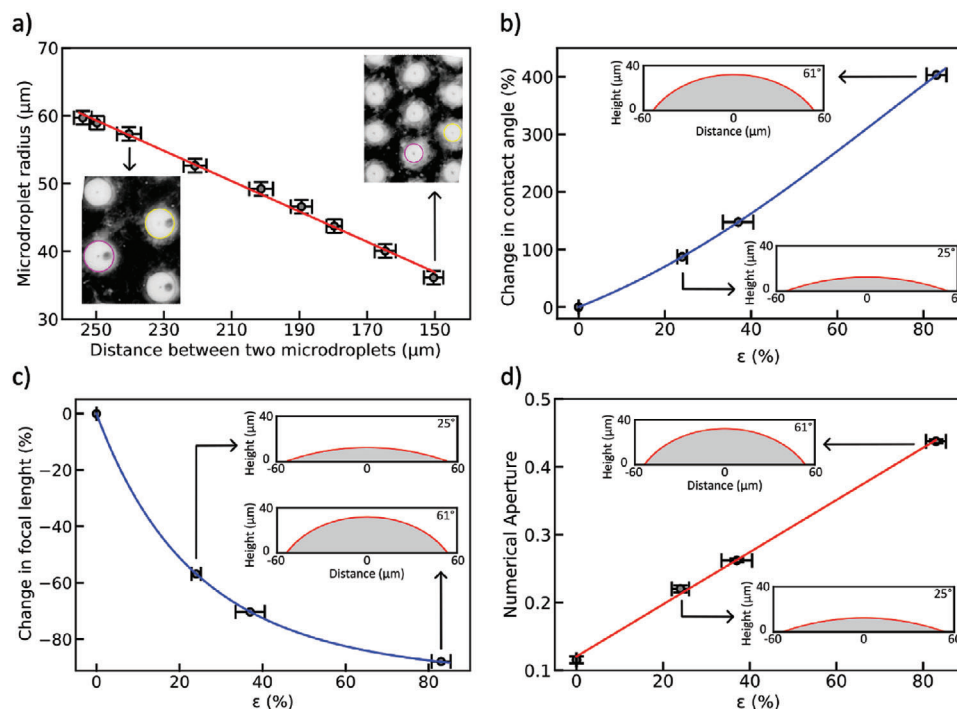


**Figure 3.** Study of microlenses' morphology at different engineering strains  $\epsilon$ . a) Plot of microdroplet radius versus distance between two adjacent microdroplets. The red solid line corresponds to a linear fit. Insets are optical micrographs of the printed microdroplets upon different values of stress release. b) Plot of the experimental change in contact angle and c) calculated paraxial focal length of the print-n-release microlenses for different values of  $\epsilon$ . The reference values were the native contact angle and focal length of a microdroplet placed on top of a non-stretched substrate, respectively. The solid blue line corresponds to the theoretical model. Insets are measured profiles of the corresponding microlenses. d) Plot of the numerical aperture of microlenses versus  $\epsilon$ . The red line corresponds to a linear fit. Insets are measured profiles of the corresponding microlenses.



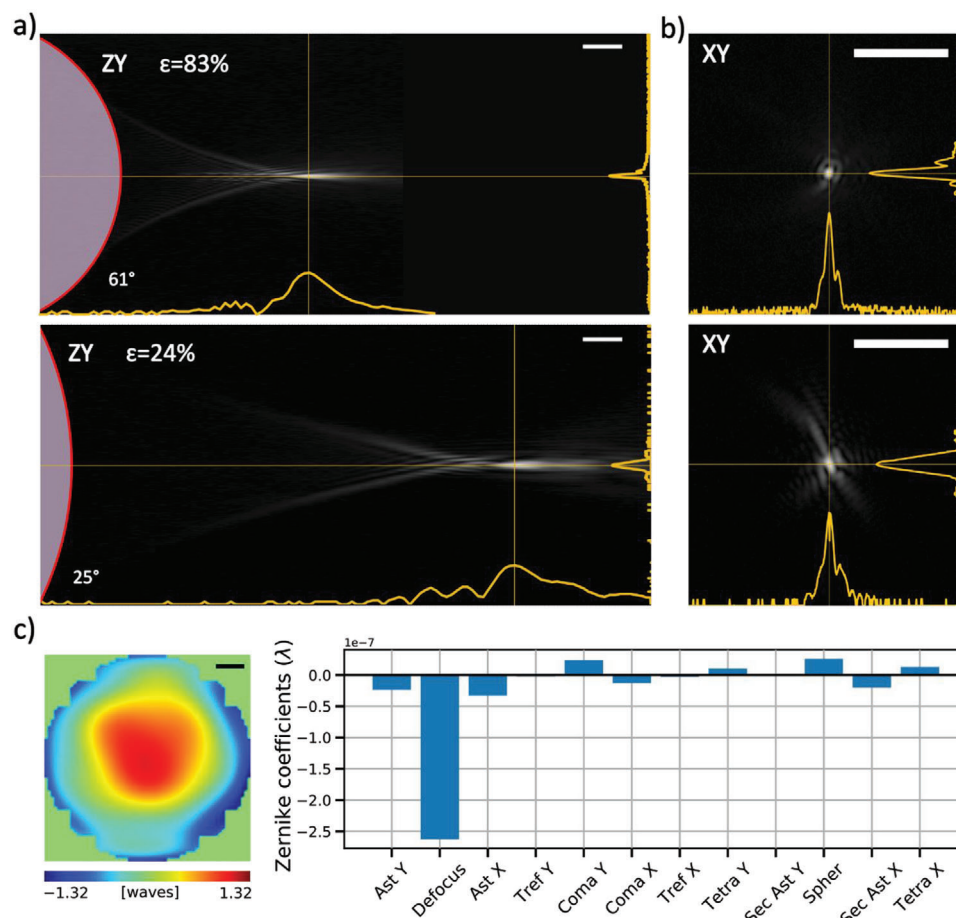


**Figure 4.** Assessment of the optical performance of microlenses fabricated with print-n-release. a) Colormaps of the intensity of a laser beam focused by a microlens with  $\epsilon = 83\%$  (top) and  $\epsilon = 24\%$  (bottom) at different positions along the propagation axis (ZY plane). The insets are intensity plots along the optical axis of each microlens and the cross-section at the focal plane. The microlens profile is also shown. Scale bars 15  $\mu\text{m}$ . b) Corresponding colormaps of the measured PSF at the focal plane. c) Reconstructed phase map of the wavefront after passing through a microlens (left). The phase change is measured in wavelengths of the incident laser light. Scale bar 15  $\mu\text{m}$ . Bar chart of Zernike coefficients (represented in wavelengths of the incident laser light) of various Zernike polynomials/aberrations (right).

in focal length, calculated using geometric optics, as a function of  $\epsilon$ . The focal length decreases with  $\epsilon$ , exhibiting the behavior theoretically predicted – see solid blue line. For instance, the microlenses fabricated at  $\epsilon = 24\%$  experimented a  $-57\%$  change in the focal length and have an average final focal length of 210  $\mu\text{m}$ . The microlenses fabricated at  $\epsilon = 83\%$  experimented a change of  $-88\%$  in focal length and have an average final focal length of 109  $\mu\text{m}$ . Importantly, the NA of the microlenses can also be controlled by adjusting  $\epsilon$  (Figure 3d). For the range of  $\epsilon$  analyzed, the calculated NA increased from a minimum value of 0.12 to 0.44 when increasing  $\epsilon$  from 0% to 83%. These results demonstrate how print-n-release allows for remarkable control in the focusing performance of the fabricated microlenses. Indeed, given the relationship between NA and the ability to confine light down to a small focal volume, the minimum focus spot size will decrease as  $1/\epsilon$  and the DOF as  $1/\epsilon^2$ .<sup>[36]</sup> In addition, our technique makes it possible to obtain microlenses with identical base diameter but different focal length thanks to the additional degree of freedom that  $\epsilon$  represents. This aspect, which is key when integrating microlenses on space-constrained systems such as

arrayed photodetectors,<sup>[37]</sup> would not be possible with traditional wet DWT.

## 4. Optical Performance

A thorough evaluation of the optical performance of the microlenses is required to validate the suitability of print-n-release. Note that, in the previous section, the focal length and numerical aperture were only calculated from the lens shape under the paraxial approximation. Spherical aberration, astigmatism, or other types of aberrations can greatly affect these calculations. To this end, we measured the intensity of a laser beam focused through different microlenses at several positions along the propagation direction Z. Figure 4a shows the retrieved intensity maps along Z for two microlenses fabricated with  $\epsilon = 83\%$  and  $\epsilon = 24\%$  that feature the same base diameter but contact angles of  $61^\circ$  and  $25^\circ$ , respectively. The former exhibits a focal length of 102  $\mu\text{m}$  (distance from the microlens flat surface to the position of maximum intensity), much shorter than the 181  $\mu\text{m}$  of the latter. Additionally, the depth-of-field of the  $\epsilon = 24\%$  is longer than for

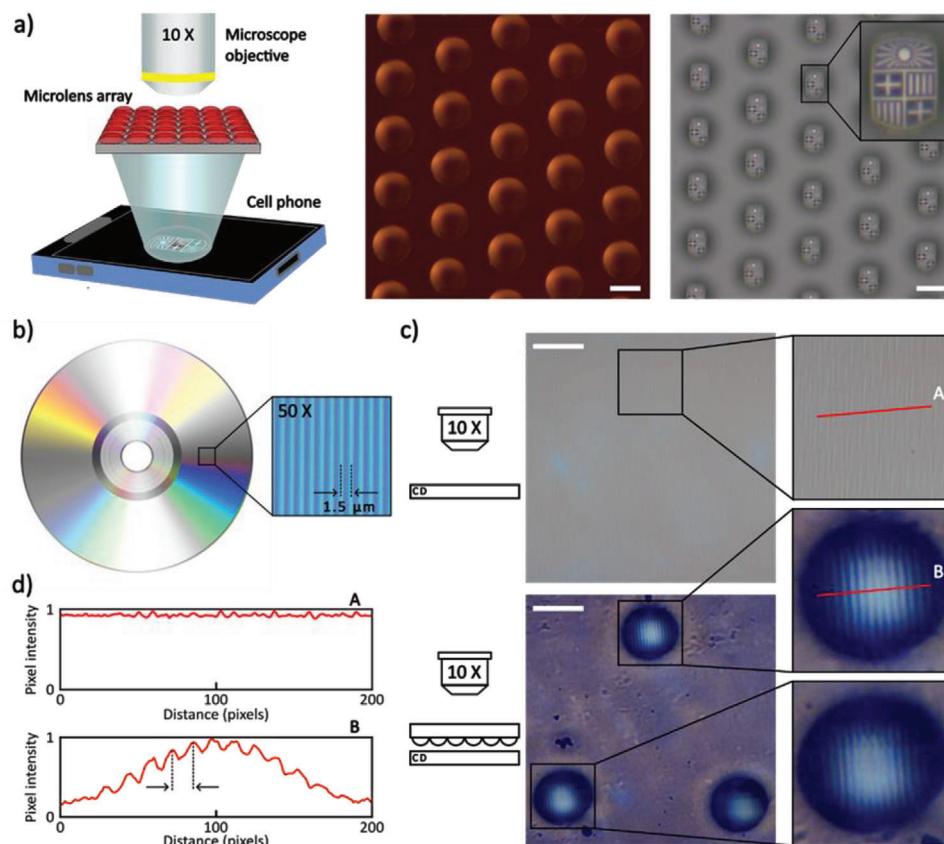


**Figure 5.** Optical imaging using print-n-release microlenses. a) Sketch of the image projection experiment (left). Optical micrographs of the microlens array (center) acquired with a 10x (0.25 NA) objective and the corresponding projected images of the Universitat de Barcelona logo (right). Scale bars 50  $\mu\text{m}$ . b) Picture of a CD. The zoom image is an optical micrograph acquired with an optical microscope with a 50X (0.5 NA) objective. c) Optical micrographs of the surface of a CD acquired with a 10X objective. Without the microlenses (top), no line can be distinguished. In contrast, by placing a microlens array close to the CD, the same objective but through microlenses (bottom), the lines can be easily observed. Scale bars 75  $\mu\text{m}$ . d) Pixel intensity profiles of the A and B lines drawn on (c) images. The A profile shows a constant value. Instead, the B profile shows a series of peaks. Each peak corresponds to a single line engraved on the CD surface.

$\varepsilon = 83\%$ , indicating a lower NA. This can be confirmed by measuring the intensity of the beam at the focal plane, also known as the focus point spread function (PSF). As shown in Figure 4b, the PSF of the microlens fabricated at  $\varepsilon = 83\%$  is more confined, with a full width at half maximum of 1.4  $\mu\text{m}$ , in contrast to the FWHM of 2.1  $\mu\text{m}$  for the  $\varepsilon = 24\%$  microlenses.

Both measured NA and focal length values agree with those calculated before from the microlens shape. These results indicate that aberrations do not play a significant role in this case. To confirm it, we measured the optical aberrations of individual microlenses using a Shack-Hartmann wavefront sensor. As shown in Figure 4c, the reconstructed phase map at the output of the microlens consists of concentric phase fringes with a high circularity. The corresponding decomposition in Zernike coefficients is also displayed. As expected for a microlens, the main component corresponds to defocus. Other aberrations are also present, but with significantly smaller contributions – at least by one order of magnitude. For example, there is some astigmatism, coma, and spherical aberration. The latter, intrinsic to spherical lenses, could explain the slight axial elongation of the focal spot observed in Figure 4a. All in all, the microlenses exhibit good optical performance, reinforcing

print-n-release as a technique for on-demand, tunable control of microlenses.

## 5. Imaging Through Microlenses

To demonstrate the imaging capabilities of the microlenses fabricated with print-n-release, we first performed an image projection experiment. We placed a microlens array some centimeters above the object to be imaged, as shown in the sketch of Figure 5a. In this case, we used the logo of the Universitat de Barcelona displayed on a cell phone screen as our object. By using a 10X microscope objective, we collected the image projected through the microlenses. Notably, a demagnified image of the original logo is formed after each microlens. The high spatial resolution of these images, with all the different elements of the logo clearly distinguishable, indicates the high quality of the so-fabricated microlenses. In addition, all projected images are in-focus, indicating that all microlenses have the same focal length. This, in turn, validates the high reproducibility and repeatability of our fabrication method.

As a final proof-of-concept, we used the microlenses to enhance the focusing performance of a low NA objective. To this

end, we imaged the periodic 1.5  $\mu\text{m}$  surface grooves of a compact disk (CD) using a bright-field microscope in transmission mode. To be able to resolve them, a 50X objective with 0.4 NA is required (Figure 5b). For lower NA objectives, the grooves remain hidden, as shown in Figure 5c. Interestingly, placing an array of print-n-release microlenses with 0.4 NA near the CD surface allows for resolving the grooves with a 10x (0.25 NA) objective. Plots of the corresponding intensity profiles further corroborate these results, as shown in Figure 5d. In this case, the microlenses form a virtual magnified image of the CD surface. Because the microlenses feature a high NA, the high-frequency components of the object are not filtered out by the microlenses. Therefore, provided a high enough magnification, image of the grooves can be resolved even with a 5x objective with NA as low as 0.15 (Figure S4, Supporting Information).

## 6. Conclusions

Print-n-release combines wet DWTs with substrate reshaping for the simple fabrication of microlenses with tailored optical properties. Specifically, it allows control of the optical properties of polymeric microlenses by simply adjusting the stress applied on the elastomeric substrate where they are fabricated. The only requirement is the use of transparent liquid prepolymers with low vapor pressure, whose contact line is pinned when printed on top of a pre-stretched substrate. Many UV-curable polymers fulfill these conditions, and some positive photoresists do as well. The additional degree of freedom that substrate reshaping represents can be used to extend the application of DWTs for microlens fabrication, breaking the constraint that the wettability of the substrate represents.

As our results demonstrate, by elongating the substrate by 80%, microlenses can be fabricated with a contact angle 400% higher than that dictated by the droplet-substrate wettability. The corresponding focal length decreases by a factor of 90%, allowing for microlenses with a high focusing power. Such behavior is in good agreement with a simple theoretical model, making print-n-release predictable. All the fabricated microlenses feature good optical quality, with low high-order aberrations. The possibility to use any wet DWTs, while maintaining the main advantages of these techniques in terms of throughput, ease of implementation and compatibility with flexible substrates, can help to close the existing gap between rapid microlens fabrication and on-demand shape selection.

## 7. Experimental Section

**Laser Direct-Write System:** The direct-write system used in the experiments herein consisted of a pulsed diode-pumped ytterbium fiber laser (Rofin Powerline F20 Varia) operated at its fundamental IR wavelength (1064 nm) combined with a galvanometric mirrors head and a f-theta lens (100 mm focal length). The VisualLaserMarker software was used to select the pulse energy, pulse length and repetition rate (from 5 to 800  $\mu\text{J}$ , 4 to 200 ns, and 2 kHz to 1 MHz, respectively) while executing 2D patterns designed digitally. The laser beam with a Gaussian intensity profile was focused on a spot of 40  $\mu\text{m}$  in diameter that could be scanned on a 6x6 cm surface at speeds between 10  $\text{mm s}^{-1}$  and 5  $\text{m s}^{-1}$ . The laser pulse energy was calibrated by using a thermopile. It was worth noticing that this setup allows an almost instantaneous LIFT printing of digitally designed

patterns of microlenses on a macroscopic surface with a user-selectable arrangement. The fabrication time was mainly limited by the UV curing time of the microlenses that was  $\approx 2$  min.

**Laser-Induced Forward Transfer:** To perform LIFT, normal printing configurations and processes were followed.<sup>[16]</sup> The donor layers were prepared by spreading a thin film of Norland Optical Adhesive 61 (Norland Products, with a refractive index of 1.56 and viscosity of 0.3 Pa·s) via blade coating on top of microscope slides covered with a 10 nm thick titanium film. Every microscope slide was previously washed with soap, rinsed with deionized water, and dried with nitrogen. The titanium layer acts as an absorbing layer because the optical adhesive was transparent to the laser radiation, with non-observable effects on the printed droplets. The donor substrate was placed above the receiver substrate with the thin donor layer facing down at a separation of  $\approx 100$   $\mu\text{m}$  by using scotch tape plus non-adhesive paper as spacers. This small gap configuration was selected to ensure close ink transfer at low energies and get small features via a stable jetting regime. The receiver substrate was a flat piece of double-sided foam tape (VHB 4910 from 3M) attached to the stretching setup that was elongated before LIFT printing. This material exhibits viscoelastic properties, allowing for elastic deformations as high as 200%. Then, the printings were performed by focusing the laser beam on the absorbing layer. After printing, the donor substrate was removed, the elongation stress was released and, finally, the microdroplets were cured under UV light exposure by using the THORLABS CS2010-UV Curing LED System.

**Stretching Setup:** A lathe chuck, originally designed to clamp workpieces in turning operations, was used to apply the pre-stretch on the receiver substrate. A circular piece of double-sided tape was cut and attached to the top part of the circular jaws when closed. Then, the jaws were concentrically and simultaneously opened with a screwdriver. The system induces a real biaxial strain on the substrate that can be approximated as isotropic in the center between the jaws. Special care must be taken when selecting the printing area, the closer to the center the more isotropic the strain is. The chuck was placed and fixed under the laser head to allow LIFT printing.

**Morphological and Optical Characterization:** An optical microscope (Carl Zeiss model AXIO Imager.A1) was used to visually inspect the printed microlenses and measure their diameter. An interferometer (Sensofar PL $\mu$  2300) was used to capture the microlenses topography. From the given topographic reconstruction, a vertical line profile passing through the center of each microlens was taken and a spherical cap model was fitted to data to calculate the contact angle and radius of curvature. The morphology of the microlenses was also visualized with a Scanning Electron Microscope (FESEM JEOL J-7100) available in the *Centres Científics i Tecnològics de la Universitat de Barcelona* (CCiTUB). The shrinking of microlenses in real-time was recorded with a CMOS camera (Thorlabs) connected to an assembled microscope.

The optical properties of the microlenses were also measured with the help of the Carl Zeiss model AXIO Imager.A1 optical microscope. The intensity profile of the laser after passing through the microlenses was recorded at different planes perpendicular to the optical axis. These profiles were used to determine their focal length. The same optical microscope was used to take images of the UB logo projected through the microlenses and to make images of lines present in a CD, with and without microlenses, to check their imaging performance. A Shack Hartmann wavefront sensor (Dynamic Optics) was used to analyze the effect of the microlenses on an incident laser light beam to characterize their optical aberrations.

## Supporting Information

Supporting Information is available from the Wiley Online Library or from the author.

## Acknowledgements

The authors acknowledge financial support from the Spanish Ministerio de Ciencia e Innovación (PID2020-112669GB-I00). Dr. Duocastella also



thanks the European Research Council (ERC) under the European Union's Horizon 2020 research and innovation programme (grant agreement No. 101002460). Dr. Duocastella is a Serra Hunter professor.

## Conflict of Interest

The authors declare no conflict of interest.

## Author Contributions

M.D. and J.M.F supervised research, E.M. performed experiments and analyzed the data. E.M. and M.D. wrote the manuscript with contributions from all authors.

## Data Availability Statement

The data that support the findings of this study are available from the corresponding author upon reasonable request.

## Keywords

direct writing, fabrications, microlens arrays, micro-optics, stretching

Received: April 12, 2023

Revised: June 27, 2023

Published online:

- [1] T. Hou, C. Zheng, S. Bai, Q. Ma, W. W. Duley, A. Hu, D. Bridges, *Appl. Opt.* **2015**, 54, 7366.
- [2] A. El Gamal, H. Eltoukhy, *IEEE Circuits Devices Mag.* **2005**, 21, 6.
- [3] Y. Chen, M. Elshobaki, Z. Ye, J. M. Park, M. A. Noack, K. M. Ho, S. Chaudhary, *Phys. Chem. Chem. Phys.* **2013**, 15, 4297.
- [4] I. Gyongy, A. Davies, B. Gallinet, N. A. W. Dutton, R. R. Duncan, C. Rickman, R. K. Henderson, P. A. Dalgarno, *Opt. Express* **2018**, 26, 2280.
- [5] R. E. Alsaigh, R. Bauer, M. P. J. Lavery, *Sci. Rep.* **2020**, 10, 8741.
- [6] S. Xiao, I. Davison, J. Mertz, *Optica* **2021**, 8, 1403.
- [7] Y. Huang, Y. Qin, P. Tu, Q. Zhang, M. Zhao, Z. Yang, *Opt. Lett.* **2020**, 45, 4460.
- [8] A. Camposeo, L. Persano, M. Farsari, D. Pisignano, *Adv. Opt. Mater.* **2019**, 7, 1800419.
- [9] W. Wang, G. Chen, Y. Weng, X. Weng, X. Zhou, C. Wu, T. Guo, Q. Yan, Z. Lin, Y. Zhang, *Sci. Rep.* **2020**, 10, 11741.
- [10] F. T. O'Neill, J. T. Sheridan, *Optik (Stuttg)* **2002**, 113, 391.
- [11] Z. D. Popovic, R. A. Sprague, G. A. N. Connell, *Appl. Opt.* **1988**, 27, 1281.
- [12] T. Scharf, W. Nakagawa, H. P. Herzig, M. T. Haq, M.-S. Kim, *Opt. Lett.* **2011**, 36, 3930.
- [13] E. Roy, B. Voisin, J. F. Gravel, R. Peytavi, D. Boudreau, T. Veres, *Microelectron. Eng.* **2009**, 86, 2255.
- [14] D. Kang, C. Pang, S. Moon Kim, H. Sung Cho, H. Sik Um, Y. Whan Choi, K. Y. Suh, D. Kang, C. Pang, S. M. Kim, K. Y. Suh, H. S. Cho, H. S. Um, Y. W. Choi, *Adv. Mater.* **2012**, 24, 1709.
- [15] P. Nussbaum, R. Völkel, H. P. Herzig, M. Eisner, S. Haselbeck, *Pure Appl. Opt.* **1997**, 6, 617.
- [16] I. S. Choi, S. Park, S. Jeon, Y. W. Kwon, R. Park, R. A. Taylor, K. Kyhm, S. W. Hong, *Microsystems Nanoeng.* **2022**, 8, 98.
- [17] H. Yu, S. Peng, L. Lei, J. Zhang, T. L. Greaves, X. Zhang, *ACS Appl. Mater. Interfaces* **2016**, 8, 22679.
- [18] J. Qian, G. F. Arends, X. Zhang, *Langmuir* **2019**, 35, 12583.
- [19] J. Aizenberg, G. Hendler, *J. Mater. Chem.* **2004**, 14, 2066.
- [20] M. Wang, W. Yu, T. Wang, X. Han, E. Gu, X. Li, *RSC Adv.* **2015**, 5, 35311.
- [21] Y. Luo, L. Wang, Y. Ding, H. Wei, X. Hao, D. Wang, Y. Dai, J. Shi, *Appl. Surf. Sci.* **2013**, 279, 36.
- [22] R. Magazine, B. van Bochove, S. Borandeh, J. Seppälä, *Addit. Manuf.* **2022**, 50, 102534.
- [23] M. Singh, H. M. Haverinen, P. Dhagat, G. E. Jabbour, *Adv. Mater.* **2010**, 22, 673.
- [24] M. S. Onses, E. Sutanto, P. M. Ferreira, A. G. Alleyne, J. A. Rogers, *Small* **2015**, 11, 4237.
- [25] A. Zolfaghari, T. Chen, A. Y. Yi, *Int. J. Extrem. Manuf.* **2019**, 1, 012005.
- [26] P. Serra, A. Piqué, *Adv. Mater. Technol.* **2019**, 4, 1800099.
- [27] S. Surdo, R. Carzino, A. Diaspro, M. Duocastella, *Adv. Opt. Mater.* **2018**, 6, 1701190.
- [28] J. Marcos Fernández-Pradas, P. Serra, *Crystals* **2020**, 10, 651.
- [29] C. Florian, S. Piazza, A. Diaspro, P. Serra, M. Duocastella, *ACS Appl. Mater. Interfaces* **2016**, 8, 17028.
- [30] S. Surdo, A. Diaspro, M. Duocastella, *Appl. Surf. Sci.* **2017**, 418, 554.
- [31] W. Feng, L. Li, X. Du, A. Welle, P. A. Levkin, *Adv. Mater.* **2016**, 28, 3202.
- [32] J. Liu, M.-J. Chang, Y. Ai, H.-L. Zhang, Y. Chen, *ACS Appl. Mater. Interfaces* **2013**, 5, 2214.
- [33] S. Surdo, S. Piazza, L. Ceseracciu, A. Diaspro, M. Duocastella, *Appl. Surf. Sci.* **2016**, 374, 151.
- [34] D. Oran, S. G. Rodrigues, R. Gao, S. Asano, M. A. Skylar-Scott, F. Chen, P. W. Tillberg, A. H. Marblestone, E. S. Boyden, *Science* **2018**, 362, 1281.
- [35] W. He, X. Ye, T. Cui, *Microsystems Nanoeng.* **2021**, 7, 88.
- [36] M. Duocastella, C. Florian, P. Serra, A. Diaspro, *Sci. Rep.* **2015**, 5, 16199.
- [37] S. Surdo, A. Diaspro, M. Duocastella, *Opt. Mater. Express* **2019**, 9, 2892.